Available online at www.sciencedirect.com
ScienceDirect
Cement & Concrete Composites 30 (2008) 266–273
Cement & Concrete Composites
www.elsevier.com/locate/cemconcomp

Mechanical and hydric properties of alkali-activated aluminosilicate composite with electrical porcelain aggregates

Lucie Zuda [a], Patrik Bayer [b], Pavel Rovnaník [b], Robert Černý [a,*]

[a] Department of Materials Engineering and Chemistry, Faculty of Civil Engineering, Czech Technical University in Prague, Thákurova 7, 166 29 Prague 6, Czech Republic
[b] Institute of Chemistry, Faculty of Civil Engineering, Brno University of Technology, Žižkova 17, 60200 Brno, Czech Republic

Received 18 July 2007; received in revised form 22 October 2007; accepted 13 November 2007
Available online 21 November 2007

Abstract

Basic mechanical and hydric properties of alkali-activated aluminosilicate composite with electrical porcelain aggregates are investigated in dependence on previous thermal load up to 1200 °C. The compressive strength is found to increase by a factor of two after heating to 1200 °C, the bending strength even by a factor of six compared to the reference measurements on specimens not subjected to any thermal treatment. Water and water vapor transport is enhanced after heating to 600 °C and more. These results can be considered as quite advantageous for a material which can supposedly be used as protective layer of current reinforced concrete structures.

Keywords: Alkali-activated aluminosilicates; Electrical porcelain; Mechanical properties; Hydric properties; Thermal load

1. Introduction

Utilization of slag is one of the possibilities how to expand the range of concrete and mortars by other materials which meet the requirements for binders and in many aspects have better properties than classical Portland cement. Granulated blast furnace slag is used as a component of blended cements. However, in this case its hydraulic properties are not fully utilized. Grinding together with clinker and gypsum leaves a part of slag grains out of later hydration reaction because they are difficult to mill. Alkali activation of granulated blast furnace slag makes possible a more suitable and more economic exploitation of its hydraulic properties.

Alkali-activated slags form high-strength materials [1]. They also exhibit remarkable high-temperature resistance which makes them perspective materials for high-temperature applications, for instance as fire protecting layers in buildings and tunnels [1]. A successful application of these materials in building structures is, however, not straightforward and requires a sufficient knowledge of their properties. This, unfortunately, was not always the case of current practice because properties of materials on the basis of alkali-activated slag were studied only relatively seldom to date. We will give some examples of currently available data in what follows for a basic orientation.

Basic mechanical properties of concrete based on alkali-activated slag were studied in detail by Byfors et al. [2], Robins et al. [3], Douglas et al. [4]. Various measured results are summarized in [5]. Collins and Sanjayan [6,7] studied the development of compressive strength of concrete based on alkali-activated slag up to about 90 days and determined 28-day values of flexural strength and Young's modulus. Bakharev et al. [8] analyzed the effect of admixtures on the compressive strength of concrete based on alkali-activated slag. Shoaib et al. [9] studied the effect of heating to 600 °C on the compressive strength of mortars on the basis of alkali-activated slag. Zuda et al. [1] measured compressive and bending strengths of alkali-activated slag mortar with quartz sand aggregates after heating to high-temperatures up to 1200 °C.

* Corresponding author. Tel.: +420 224354429; fax: +420 224354446.
E-mail address: cernyr@fsv.cvut.cz (R. Černý).

0958-9465/$ - see front matter © 2007 Elsevier Ltd. All rights reserved.
doi:10.1016/j.cemconcomp.2007.11.003

Among the hydric properties of concrete based on alkali-activated slag, mostly water permeability was measured [10]. Concerning other transport parameters, Robins et al. [3] measured air permeability in concrete based on alkali-activated slag by the Figg test. Byfors et al. [2], Douglas et al. [4], Shi [10] and Roy et al. [11] studied chloride diffusion in concretes and pastes based on alkali-activated slag and on its blend with cement. Černý et al. [12] determined moisture diffusivity, sorption isotherms and water vapor diffusion resistance factor of alkali-activated slag mortar with quartz sand aggregates.

In this paper, basic mechanical and hydric properties of an alkali-activated aluminosilicate composite with electrical porcelain aggregates, namely compressive and bending strengths, moisture diffusivity, water vapor diffusion coefficient and adsorption and desorption isotherms are determined on the samples subjected to thermal loads of 200, 400, 600, 800, 1000 and 1200 °C and compared to the reference material data.

Table 1
Chemical composition of applied slag

SiO_2 (%)	Fe_2O_3 (%)	Al_2O_3 (%)	CaO (%)	MgO (%)	MnO (%)	Cl^- (%)	Na_2O (%)	K_2O (%)	SO_3 (%)
38.6	0.52	7.22	38.77	12.90	0.50	0.06	0.21	0.38	0.36

Table 2
Slag granulometry

Sieve residue		Specific surface (cm^2/g)
0.045 mm (%)	0.09 mm (%)	
12.4	1.9	3920

Table 3
Chemical composition of electrical porcelain

SiO_2 (%)	Fe_2O_3 (%)	Al_2O_3 (%)	CaO (%)	MgO (%)	Na_2O (%)	K_2O (%)	TiO_2 (%)
48.6	0.8	45.4	0.3	0.2	1.0	2.9	0.7

2. Materials and samples

Fine-ground slag of Czech origin (Kotouč Štramberk, Ltd., CZ) was used for sample preparation. Its chemical composition is shown in Table 1, its granulometry in Table 2. As alkali-activator, water glass solution was used. It was prepared using Portil-A dried sodium silicate preparative (Cognis Iberia, s.l., Spain) with silicate modulus $M_s = 1.95$ (composition: 50.8% SiO_2, 26.8% Na_2O).

Electrical porcelain provided by P-D Refractories CZ, Velké Opatovice, was used instead of commonly used sand aggregates, because of its more convenient high-temperature properties. Its porosity was 0.3% by mass, water

Table 4
Electrical porcelain granulometry

Sieve mesh (mm)	4.00	2.50	1.00	0.50	0.25	0.125	0.090	0.063	0.045
Total sieve residue (%)									
0–1 mm fraction	–	–	0.69	45.24	70.76	89.98	93.4	98.99	99.99
1–3 mm fraction	–	4.12	78.33	99.57	99.94	99.94	99.95	98.98	100.00
3–6 mm fraction	69.31	95.52	99.97	99.98	99.99	100.00	–	–	–

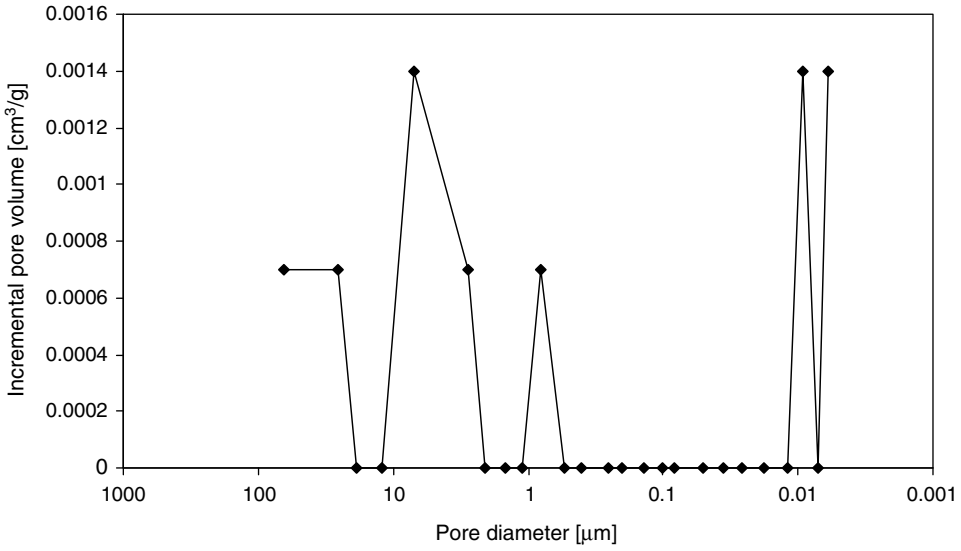

Fig. 1. Pore distribution curve of electrical porcelain.

Table 5
Composition of mixture for sample preparation

Electrical porcelain (g)			Slag (g)	Alkali-activation silicate admixture (g)	Water (ml)
0–1 mm fraction	1–3 mm fraction	3–6 mm fraction			
450	450	450	450	90	190

absorption at saturation 0.1% by mass, bulk density 2350 kg m^{-3}, thermal conductivity 2.5 W m^{-1} K^{-1}, specific heat capacity 755 J kg^{-1} K^{-1} and thermal expansion coefficient 5.1×10^{-6} K^{-1} (20–1000 °C). Chemical composition of the electrical porcelain is given in Table 3, its granulometry in Table 4 and its pore distribution curve in Fig. 1.

The composition of the mixture for sample preparation is presented in Table 5. The technology of sample preparation was as follows. First, the silicate preparative was mixed with water. The solution was then mixed in the homogenized slag-electrical porcelain mixture using a planetary mixer with the mixing rate of about 70 rpm. The final mixture was put into molds and vibrated. The specimens were demolded after 24 h and then stored for further 27 days in pure-water bath at laboratory temperature.

After the 28-days curing period, the specimens were dried at 110 °C and after drying subjected to thermal load. Heating of the samples to the predetermined temperature was always done with the rate of 10 K/min, then the specimens remained at that temperature for the time period of two hours and finally they were slowly cooled. The chosen pre-heating temperatures were 200, 400, 600, 800, 1000 and 1200 °C.

In the experimental work, the following samples were used for every pre-treatment: basic properties – 3 specimens $50 \times 50 \times 23$ mm, bending strength – 3 specimens $40 \times 40 \times 160$ mm, compressive strength – remainders of the specimens after bending test, water absorption – 3 specimens $50 \times 50 \times 23$ mm, sorption isotherms – 15 specimens $20 \times 20 \times 10$ mm. The samples for determination of water absorption were provided on all lateral sides by water- and vapor-proof plastic foil insulation.

3. Experimental methods

3.1. Basic characteristics

The water vacuum saturation method [13] was used for the measurements of bulk density, matrix density and open porosity. Each sample was dried in a drier to remove majority of the physically bound water. After that the samples were placed into the desiccator with deaired water. During three hours air was evacuated with vacuum pump from the desiccator. The specimen was then kept under water not less than 24 h.

From the mass of the dry sample m_d, the mass of water saturated sample m_w, and the mass of the immersed water saturated sample m_a, the volume V of the sample was determined from the equation

$$V = \frac{m_w - m_a}{\rho_l}, \tag{1}$$

where ρ_l is the density of water. The open porosity ψ_0, the bulk density ρ and the matrix density ρ_{mat} were calculated according to the equations

$$\psi_0 = \frac{m_w - m_d}{V\rho_l}, \tag{2}$$

$$\rho = \frac{m_d}{V}, \tag{3}$$

$$\rho_{mat} = \frac{m_d}{V(1-\psi)}. \tag{4}$$

Mercury intrusion porosimetry (MIP) measurements were used for determination of pore distribution in the range of 300 μm to 0.006 μm. They were performed using the porosimeter Micromeritics POREZISER 9310 with maximum working pressure of 200 MPa.

Scanning electron microscopy (SEM) was the method chosen for basic characterization of structural changes after thermal loading. The scanning electron microscope JEOL JSM-U3 with 10 nm resolution was used.

3.2. Mechanical properties

The compressive strength and bending strength were determined as the mechanical properties most characteristic for aluminosilicates. The bending strength was measured by the standard three-point bending test using a 500 kN testing device. The size of the specimens was chosen in accordance to the sample dimensions common in testing cement mortars. Every specimen was positioned in such a way that the sides which were horizontal during the preparation were in the vertical position during the test. The compressive strength was determined by a compression test using the same device. It was done on the parts of the specimens broken at the bending test. The specimens were placed between the two plates of the testing device in such a way that their lateral sides adjoining during the preparation to the vertical sides of the molds were in contact with the plates. In this way, the imprecision of the geometry on the upper cut off side was not affecting negatively the experiment.

3.3. Water absorption and moisture diffusivity

Water absorption was analyzed using a standard experimental setup. The specimen was water and vapor-proof insulated on four lateral sides and the face side was immersed 1–2 mm in the water. Constant water level in

tank was achieved by a Marriott bottle with two capillary tubes. One of them, inside diameter 2 mm, was ducked under the water level, the second one, inside diameter 5 mm, was above water level. The automatic scale allowed for recording the increase of mass. The water absorption coefficient A (kg m^{-2} s$^{-1/2}$) was then calculated using the formula

$$i = A \cdot \sqrt{t}, \tag{5}$$

where i is the cumulative water absorption (kg m^{-2}), t the time from the beginning of the suction experiment. The water absorption coefficient was then used for calculation of the apparent moisture diffusivity [14]

$$\kappa_{app} \approx \left(\frac{A}{w_c - w_0}\right)^2, \tag{6}$$

where w_c is the saturated moisture content (kg m^{-3}) and w_0 the initial moisture content (kg m^{-3}).

3.4. Water vapor transport parameters

The cup method was used for determination of water vapor transport parameters. The measurement was carried out in steady state under isothermal conditions, using one-dimensional water vapor diffusion setup, determination of water vapor diffusion flux through the specimen and measuring partial water vapor pressure in the air under and above specific specimen surface.

Two versions of the cup method were employed in the measurements of water vapor diffusion coefficient. In the first one (dry cup), the sealed cup containing burnt $CaCl_2$ (5% relative humidity) was placed in a controlled climatic chamber at 25 ± 0.5 °C and 35% relative humidity and weighed periodically. In the second one (wet cup), the cup containing saturated K_2SO_4 solution (97% relative humidity) was placed in 25 ± 0.5 °C and 25% relative humidity environment. The sealed cups with samples were weighed periodically. The steady state values of mass gain or mass loss were utilized for the determination of water vapor transport properties.

The water vapor diffusion coefficient D (m^2 s^{-1}) was calculated from the measured data according to the equation

$$D = \frac{\Delta m \cdot d \cdot R \cdot T}{S \cdot \tau \cdot M \cdot \Delta p_p}, \tag{7}$$

where Δm is the amount of water vapor diffused through the sample (kg), d the sample thickness (m), S the specimen surface (m^2), τ the period of time corresponding to the transport of mass of water vapor Δm (s), Δp_p the difference between partial water vapor pressure in the air under and above specific specimen surface (Pa), R the universal gas constant (J mol^{-1} K^{-1}), M the molar mass of water (kg mol^{-1}), T the absolute temperature (K).

On the basis of the diffusion coefficient, the water vapor diffusion resistance factor μ (−) was determined,

$$\mu = \frac{D_a}{D}, \tag{8}$$

where D_a is the diffusion coefficient of water vapor in the air (m^{2}s^{-1}).

3.5. Adsorption and desorption isotherms

In the measurements of adsorption isotherms the samples were placed into the desiccators with different solutions to simulate different values of relative humidity [13]. The initial state for all the measurements was dry material. The experiment was performed parallel in all desiccators in a common way. The mass of samples was measured in specified periods of time until steady state value of mass was achieved. Then, the moisture content by mass was calculated. The desorption isotherms were determined in a similar way, only the initial state was material with maximum hygroscopic moisture content.

4. Experimental results and discussion

4.1. Basic characteristics

Table 6 shows the basic characteristics of the studied aluminosilicate material determined by water vacuum saturation method after thermal load. The porosity and bulk density were changed only moderately for heating up to 600 °C. However, heating to 800 and 1000 °C led to an up to 10% decrease of bulk density and up to 40% increase of porosity in comparison with the reference room-temperature data. This indicates structural changes and/or chemical reactions in the material. After heating to the temperature of 1200 °C the studied material exhibited very similar basic properties to those at room temperature.

The global characteristics of the porous space determined by mercury intrusion porosimetry (Table 7) exhibited – as for the effect of thermal treatment – similar qualitative features to the porosities measured by water vacuum saturation method. The major changes appeared for heating to 800 and 1000 °C. However, the values of porosity found out by mercury porosimetry were systematically lower than those obtained by water vacuum saturation method. This may indicate presence of pores bigger than 100 μm or major cracks.

Table 6
Basic properties of the studied composite measured by water vacuum saturation method in dependence on thermal load

Thermal load (°C)	Bulk density (kg/m^3)	Matrix density (kg/m^3)	Porosity (m^3/m^3)
25	2101	2659	0.21
200	2184	2853	0.23
400	2105	2756	0.24
600	2164	2860	0.24
800	1977	2726	0.28
1000	1948	2752	0.29
1200	2117	2685	0.21

Table 7
Basic properties of the studied composite measured by mercury intrusion porosimetry in dependence on thermal load

Thermal load (°C)	Total intrusion volume (cm^3/g)	Total pore area (m^2/g)	Median pore diameter (μm)	Bulk density (g/cm^3)	Porosity (m^3/m^3)
20	0.059	3.96	3.46	1.27	0.075
200	0.080	6.62	4.04	2.06	0.16
400	0.059	3.41	5.84	2.24	0.13
600	0.071	10.48	1.46	2.20	0.16
800	0.125	0.82	2.61	2.06	0.26
1000	0.164	1.09	2.31	1.88	0.30
1200	0.049	3.33	33.6	2.45	0.12

The pore distribution curves in Fig. 2 show that the apparent reason for porosity increase after heating to 800 and 1000 °C was the appearance of very distinct double peak between 1 μm and 10 μm. The volume of pores in this range increased more than five times compared to the specimens heated to lower temperatures. However, this peak was completely missing after heating to 1200 °C and a new peak between 10 and 100 μm appeared instead. This indicates major structural changes between 1000 and 1200 °C.

SEM micrographs in Figs. 3–5 confirm well the results of porosimetric measurements. The reference specimen in Fig. 3 show relatively compact structure with small cracks about 1–2 μm wide. The high amount of pores in the range of 1–10 μm observed in MIP measurements was clearly visible in Fig. 4 representing the specimen heated to 800 °C. After heating to 1200 °C the microstructure was changed completely as it is demonstrated in Fig. 5.

One of the reasons for the observed changes in pore distribution and in the character of microstructure was crystallization of akermanite $Ca_2MgSi_2O_7$ and the subsequent growth of its crystals after heating to higher temperatures. This was already proven in previous investigations using XRD method in [1]. The sudden change in the microstructure between 1000 and 1200 °C may, however, be also related to the use of electrical porcelain aggregate. Electrical porcelain is produced at the temperature of approximately 1400 °C, but its stability in alkali environment is only up to 1150 °C. At higher temperature it starts to melt and forms a ceramic bond with an AAS matrix [15].

4.2. Mechanical properties

Table 8 presents compressive and bending strengths in dependence on thermal load. The results of compressive strength measurements were in good qualitative agreement with the changes in porosity and bulk density in Table 6. The compressive strength minima were achieved after heating to 800 and 1000 °C, but for the heating temperature of 1200 °C the compressive strength increased almost two times in comparison with the room temperature measurement. The changes in bending strength were up to 1000 °C loading temperature not very dramatic, the decrease was 20% in maximum. However, heating to

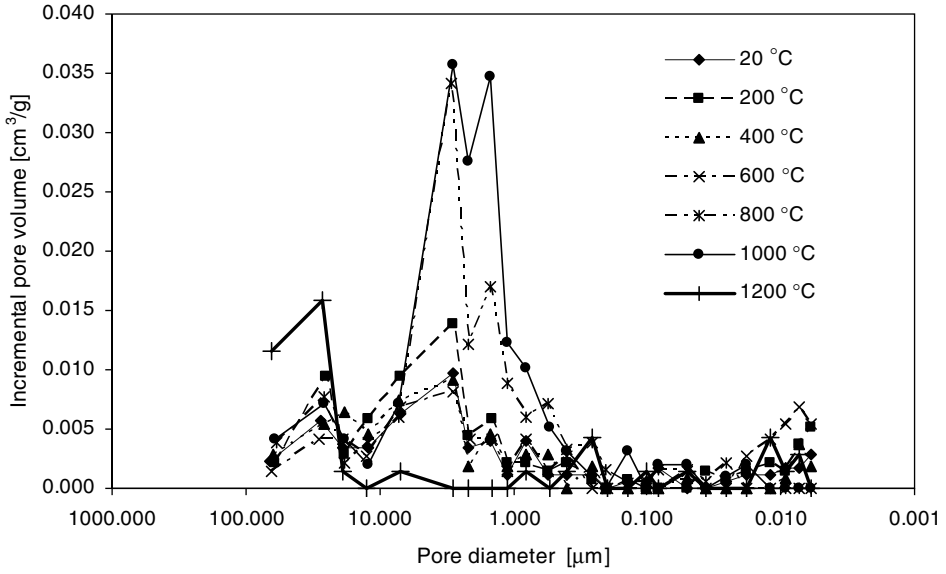

Fig. 2. Pore distribution curves of the studied alkali-activated aluminosilicate in dependence on thermal load.

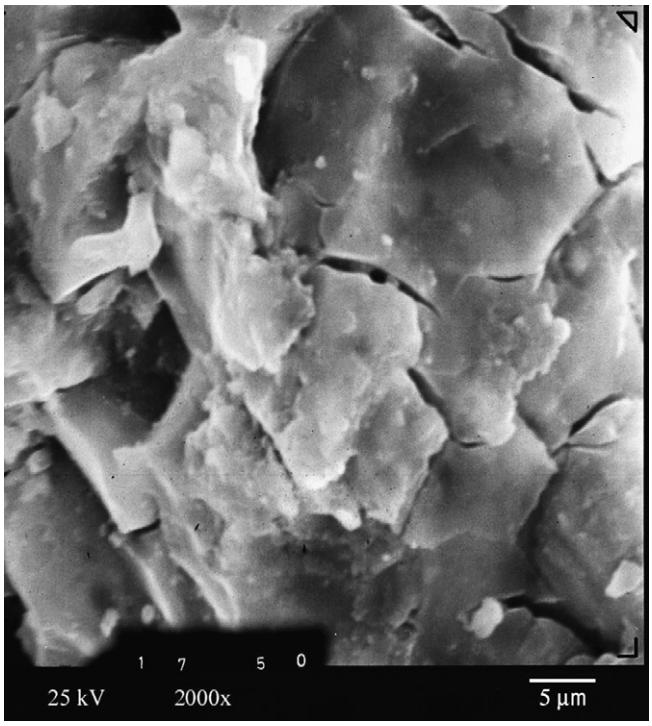

Fig. 3. SEM image of the reference specimen.

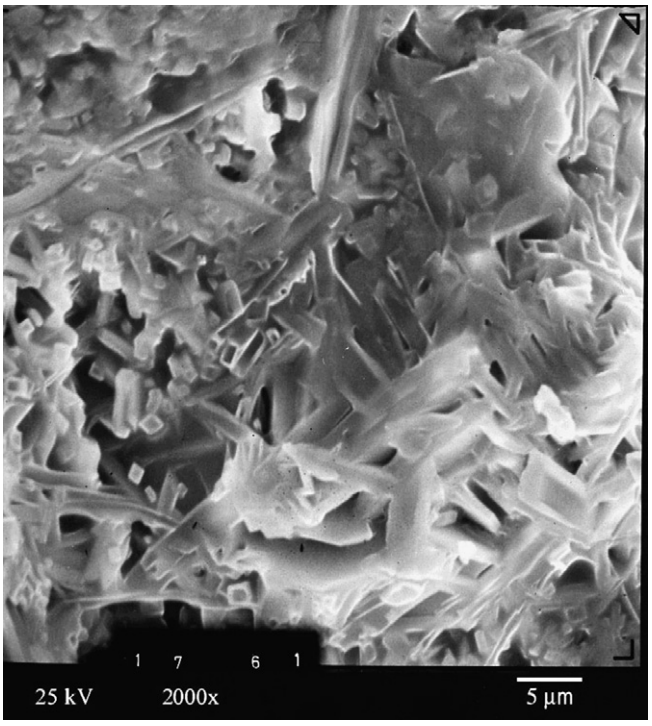

Fig. 5. SEM image of the studied alkali-activated aluminosilicate after heating to 1200 °C.

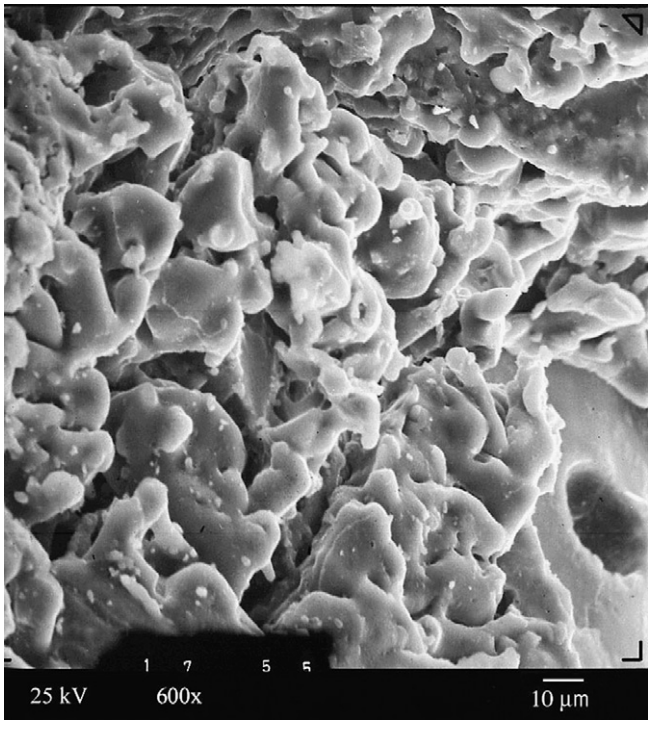

Fig. 4. SEM image of the studied alkali-activated aluminosilicate after heating to 800 °C.

Table 8
Mechanical properties

Thermal load (°C)	Bending strength (MPa)	Compressive strength (MPa)
25	3.7	49.9
200	3.6	49.7
400	3.1	39.1
600	3.0	32.6
800	3.4	15.7
1000	3.7	19.1
1200	21.4	95.3

1200 °C led to a very significant increase of bending strength which was six times higher than at room temperature.

In comparison with the results obtained for similar composite with quartz sand aggregates in [1], the mechanical properties of the composite with electrical porcelain aggregates were clearly superior. While the values of compressive and bending strengths for heating up to 600 °C were comparable for the two composites, the decrease in strengths after heating to 800 °C was for the composite with electrical porcelain aggregates not that significant as in the case of the composite with quartz sand aggregates. This seems to be the effect of electrical porcelain which does not exhibit any significant volumetric changes up to 1150 °C. Quartz, on the other hand, changes its molar volume at 573 and 870 °C.

The fortification of the porous structure after heating to 1200 °C was for the composite with electrical porcelain aggregates much more remarkable than for that with quartz sand aggregates (where the mechanical strengths achieved similar values to reference specimens, see [1]). This was, in addition to the previously observed crystallization

of akermanite, clearly a consequence of formation of new crystalline phases, wollastonite, enstatite, and gehlenite as a result of melting of electrical porcelain in the presence of alkalis (see [16] for details).

4.3. Hydric properties

The apparent moisture diffusivity determined using the water absorption experiment is given in Table 9. It increased already from 600 °C loading temperature but then it was stabilized at almost constant values roughly corresponding to moisture diffusivity of ceramic brick. This can be considered as a very good result. Water vapor diffusion resistance factor decreased with increased loading temperature only moderately, 30% in maximum and for 1200 °C it slightly increased. This roughly corresponds with the porosity data in Table 6.

Fig. 6 shows that with increasing temperature the water vapor adsorption capacity decreased relatively fast so that after heating to 800 °C almost negligible amount of water vapor was adsorbed on the pore walls of the studied specimen. The water vapor adsorption increased then for 1000 and 1200 °C heating temperatures, but the absorbed amount of moisture was four to five times lower than for reference specimens. This indicates important changes in pore distribution, namely a significant decrease of pore surface area after heating to 800 °C and its subsequent increase after heating to 1000 and 1200 °C. These findings are in good agreement with MIP results in Table 7. The sorption hysteresis was in an expected range.

Table 9
Hydric properties

Thermal load (°C)	Water vapor diffusion resistance factor (−)		Apparent moisture diffusivity (10^{-6} m^2 s^{-1})
	Dry cup	Wet cup	
25	25	12	0.28
200	22	12	0.10
400	22	11	0.21
600	20	10	0.39
800	18	10	0.35
1000	17	10	0.32
1200	19	11	0.34

5. Conclusions

The alkali-activated aluminosilicate composite with electrical porcelain aggregates investigated in this paper exhibited very convenient behavior after being subjected to high temperatures. The most important results were achieved for mechanical properties. The compressive strength of the studied aluminosilicate increased by a factor of two after heating to 1200 °C and the bending strength even by a factor of six compared to the reference measurements on specimens not subjected to any thermal load. These are quite superior results.

Water and water vapor transport were enhanced after heating to 600 °C and more. This seems to be an advantage for a material which might supposedly be used in the form of protective layers for the current reinforced concrete structures. Faster water transport in a structure exposed to high temperatures can possibly reduce the damage induced by water evaporation and the accompanying pore pressure increase.

Therefore, it can be concluded that the studied alkali-activated aluminosilicate composite with electrical porcelain aggregates has a good potential for future use in building industry in such applications where high-temperature protection is necessary, i.e., just in the application field where traditional cement based materials fail.

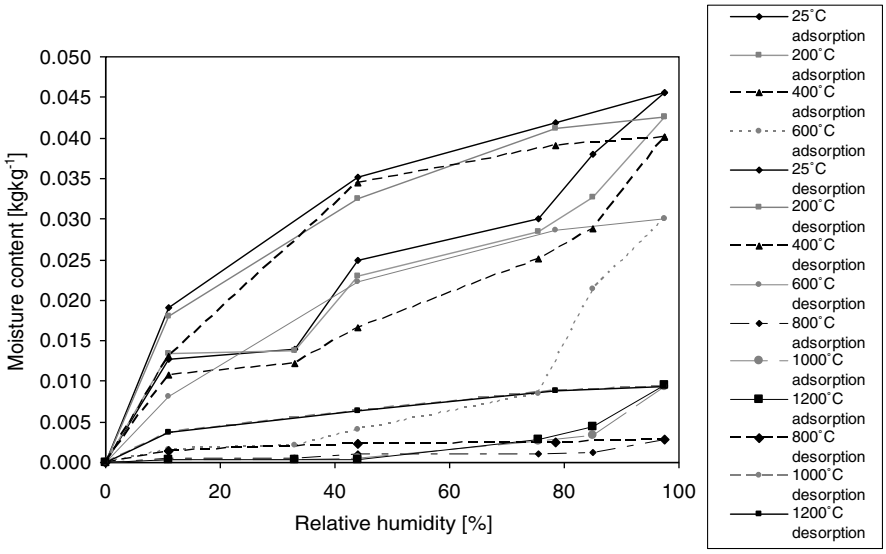

Fig. 6. Adsorption and desorption isotherms of the studied alkali-activated aluminosilicate.

Acknowledgements

This research was supported by the Ministry of Education, Youth and Sports of Czech Republic, under Project No. MSM: 6840770031.

References

[1] Zuda L, Pavlík Z, Rovnaníková P, Bayer P, Černý R. Properties of alkali-activated aluminosilicate material after thermal load. Int J Thermophys 2006;27:1250–63.
[2] Byfors K, Klingstedt G, Lehtonen V, Pyy H, Romben L. Durability of concrete made with alkali-activated slag. ACI SP Proc 1989;114: 1429–68.
[3] Robins PJ, Austin SA, Issaad A. Suitability of GGBFS as a cement replacement for concrete in hot arid climates. Mater Struct 1992;25:598–612.
[4] Douglas E, Bilodeau A, Malhotra VM. Properties and durability of alkali-activated slag concrete. ACI Mater J 1992;89:509–16.
[5] Wang SD, Pu XC, Scrivener KL, Pratt PL. Alkali-activated slag cement and concrete: a review of properties and problems. Adv Cem Res 1995;7:93–102.
[6] Collins FG, Sanjayan JG. Workability and mechanical properties of alkali-activated slag concrete. Cem Concr Res 1999;29:455–8.
[7] Collins FG, Sanjayan JG. Strength and shrinkage properties of alkali-activated slag concrete placed into a large column. Cem Concr Res 1999;29:659–66.
[8] Bakharev T, Sanjayan JG, Cheng YB. Effect of admixtures on properties of alkali-activated slag concrete. Cem Concr Res 2000;30:1367–74.
[9] Shoaib MM, Ahmed SA, Balaha MM. Effect of fire and cooling mode on the properties of slag mortars. Cem Concr Res 2001;31:1533–8.
[10] Shi C. Strength, pore structure and permeability of alkali-activated slag mortars. Cem Concr Res 1996;26:1789–99.
[11] Roy DM, Jiang W, Silsbee MR. Chloride diffusion in ordinary, blended and alkali-activated cement pastes and its relation to other properties. Cem Concr Res 2000;30:1879–84.
[12] Černý R, Zuda L, Drchalová J, Toman J, Rovnaníková P, Bayer P. Hygric and thermal properties of an alkali-activated aluminosilicate material. In: Fazio P, Rao H, Ge J, Desmarais G, editors. Research in building physics and building engineering. London: Taylor and Francis; 2006. p. 35–42.
[13] Roels S, Carmeliet J, Hens H, Adan O, Brocken H, Černý R, et al. Interlaboratory comparison of hygric properties of porous building materials. J Therm Envelop Build Sci 2004;27:307–25.
[14] Černý R, Poděbradská J, Drchalová J. Water and water vapor penetration through coatings. J Therm Envelop Build Sci 2002;26:165–77.
[15] Bayer P. Modification of properties of composite based on aluminosilicate matrix. Ph.D. thesis, Brno: FCE BUT; 2005.
[16] Rovnaníková P, Bayer P, Rovnaník P, Novák J. Properties of alkali-activated aluminosilicate materials with fire-resistant aggregate after high-temperature loading. In: Dhir RK, Harrison TA, Newlands MD, editors. Cement combinations for durable concrete. Dundee: Thomas Telford; 2005. p. 277–86.